JOURNAL OF GEOPHYSICAL RESEARCH, VOL. 111, B06409, doi:10.1029/2005JB003987, 2006

Bending-like behavior of thin wedge-shaped elastic fault blocks

Yan Hu[1] and Kelin Wang[1,2]

Received 6 August 2005; revised 12 January 2006; accepted 17 March 2006; published 27 June 2006.

[1] We derive an Airy stress function solution for a submarine or subareal, infinite or finite, elastic wedge with a frictional basal fault. The solution has a simple compact expression and has corrected errors present in earlier elastic wedge solutions. We use the solution to study frequently observed bending-like behavior of relatively thin wedges, in which lateral tension and compression coexist but are vertically partitioned. Conditions to cause such coexistence are best understood by examining how the position of a neutral line changes in response to variations in basal traction, pore fluid pressure, and wedge geometry. We have used the example of the Mauna Loa–Kilauea rift flank in Hawaii to illustrate how the solution may be applied to geological problems. Our results generally support the concept of a "bent" elastic wedge previously proposed to explain coeval normal faulting in the upper part and reverse faulting in the lower part of the rift flank. However, we find that coexistence of tension and compression in a wedge of this type can occur over a much wider range of pore fluid pressure values and basal friction conditions than previously thought and does not require unusual geological processes.

Citation: Hu, Y., and K. Wang (2006), Bending-like behavior of thin wedge-shaped elastic fault blocks, *J. Geophys. Res.*, *111*, B06409, doi:10.1029/2005JB003987.

1. Introduction

[2] Wedge-shaped geological bodies are widely present at all scales, from the hanging walls of any dipping faults to accretionary prisms and thrust orogenic belts. The mechanics of a wedge-shaped block with a frictional basal boundary is thus of great interest and importance. Over the past two decades, a number of models have been used to study wedge mechanics. Analytical stress solutions have been obtained for elastic wedges [*Yin*, 1993; *Yin and Kelty*, 2000], viscous wedges [*Platt*, 1993], and critically tapered Coulomb (plastic) wedges [*Davis et al.*, 1983; *Dahlen*, 1984, 1990]. Some numerical models have also dealt with the mechanics of wedge-shaped bodies with frictional basal faults [e.g., *Wang and He*, 1999].

[3] An elastic wedge is one of the most relevant models for studying coeval lateral tension and compression in fault blocks. Relative to an initial reference stress state, an incremental change in normal and/or shear traction along the basal fault may generate whole wedge tension, whole wedge compression, or coexistent tension and compression that are vertically partitioned. Because the coexistence of tension and compression is similar to that in a flexed elastic plate (beam), we call it bending-like behavior. In this paper, we present a new analytical solution for a uniform elastic wedge and investigate conditions for the bending-like behavior. Our work was inspired by the pioneer efforts of *Yin* [1993] and *Yin and Kelty* [2000]. With a more rigorous formulation and solution of the mechanical problem, we were able to expand their work by ironing out errors, providing a compact form, more thoroughly exploring the parameter space, and reanalyzing a previously studied example from the Mauna Loa–Kilauea rift flank in Hawaii.

2. A Stress Function Solution

2.1. Infinite Elastic Wedge

[4] The formulation of our problem is identical to that of *Dahlen* [1984] for a critically tapered Coulomb wedge except that our wedge is elastic. We consider an infinite wedge with a surface slope angle α and basal dip β subject to gravitational body force ρg, where ρ and g are the density of the wedge material and gravitational acceleration, respectively (Figure 1a). For a submarine wedge, water load at the upper surface is $\rho_w g D$, where ρ_w is water density, and $D = D_0 - x \sin \alpha$ is water depth above the upper surface, with D_0 being the depth at the toe of the wedge ($x = y = 0$). The solution presented here can be used for a subareal wedge if we let $\rho_w = 0$.

[5] Assuming plane strain, the stress equilibrium equations are as follows:

$$\frac{\partial \sigma_x}{\partial x} + \frac{\partial \tau_{xy}}{\partial y} - \rho g \sin \alpha = 0 \tag{1a}$$

$$\frac{\partial \tau_{xy}}{\partial x} + \frac{\partial \sigma_y}{\partial y} + \rho g \cos \alpha = 0 \tag{1b}$$

where $-\rho g \sin\alpha$ and $\rho g \cos\alpha$ are the x and y components of ρg, respectively. Tensile normal stress is defined to be

[1]School of Earth and Ocean Sciences, University of Victoria, Victoria, British Columbia, Canada.
[2]Pacific Geoscience Centre, Geological Survey of Canada, Sidney, British Columbia, Canada.

0148-0227/06/2005JB003987$09.00

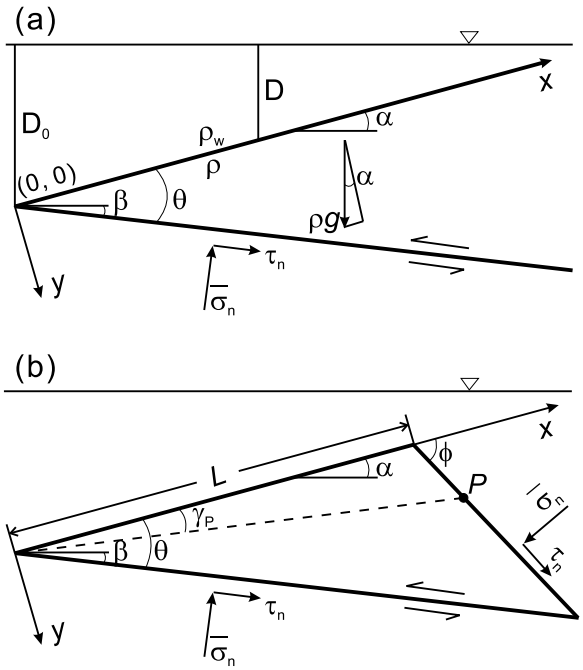

Figure 1. (a) Schematic illustration of an infinite elastic wedge to show the coordinate system (x, y), angles α and β, water depth D, and basal boundary tractions. (b) Same as Figure 1a except for a finite elastic wedge with its back at angle ϕ with the upper surface. Dashed line is the pivot line, and P is the pivot point.

positive in this work. We wish to find Airy stress function $\Phi(x, y)$ from which stresses in the wedge can be derived as follows [e.g., *Fung*, 1965]:

$$\sigma_x = \frac{\partial^2 \Phi}{\partial y^2} + \rho g x \sin\alpha \tag{2a}$$

$$\sigma_y = \frac{\partial^2 \Phi}{\partial x^2} - \rho g y \cos\alpha \tag{2b}$$

$$\tau_{xy} = -\frac{\partial^2 \Phi}{\partial x \partial y} \tag{2c}$$

[6] Following *Dahlen* [1984], we assume a constant generalized Hubbert-Rubey fluid pressure ratio λ in the wedge defined as

$$\lambda = \frac{P_f - \rho_w g D}{-\sigma_y - \rho_w g D} \tag{3a}$$

where P_f is pore fluid pressure in the wedge, and we have

$$P_f = -\lambda \sigma_y + (1-\lambda)\rho_w g D \tag{3b}$$

The relationship between stress σ and effective stress $\bar{\sigma}$ is

$$\begin{cases} \bar{\sigma}_x = \sigma_x + P_f \\ \bar{\sigma}_y = \sigma_y + P_f \end{cases} \tag{4}$$

[7] The boundary condition along the upper surface ($y = 0$) is simply pressure due to the weight of the water column above, that is,

$$\sigma_y\big|_{y=0} = -\rho_w g D = -\rho_w g D_0 + \rho_w g x \sin\alpha \tag{5a}$$

$$\tau_{xy}\big|_{y=0} = 0 \tag{5b}$$

The basal boundary ($y = x\tan\theta$, where $\theta = \alpha + \beta$) is assumed to be a planar fault to which a static friction law $|\tau_n| = |\mu_b(\sigma_n + P_f^b)|$ applies, where τ_n and σ_n are shear and normal tractions, respectively, P_f^b is pore fluid pressure along the basal fault, and $\mu_b = \tan\varphi_b$ is the coefficient of basal friction with φ_b being the angle of basal friction. Also following *Dahlen* [1984], we define an effective coefficient of basal friction

$$\mu_b' = \tan\varphi_b' = \frac{\mu_b''}{1-\lambda} \tag{6}$$

where μ_b'' is a basal friction property that depends on both μ_b and P_f^b. If a basal fluid pressure ratio λ_b similar to λ in physical meaning is properly defined, we can have

$$\mu_b'' = (1-\lambda_b)\mu_b \tag{7}$$

If we define thrust-type shear traction (for $\beta > 0$) to be positive as shown in Figure 1, and because $\bar{\sigma}_n \le 0$, the static friction law along this boundary can be rewritten as

$$\tau_n = -\mu_b'(\sigma_n + P_f) = -\mu_b'\bar{\sigma}_n \tag{8}$$

Here effective normal traction on the boundary is represented by the effective normal stress just above the basal fault. If the basal boundary (for $\beta > 0$) is a normal fault, we can use the same expression for the shear traction by allowing negative values for μ_b.

[8] For a uniform critically tapered Coulomb wedge, it can be shown that basal traction is a linear function of distance [e.g., *Davis et al.*, 1983; *Dahlen*, 1984]. The linearity is a consequence of the absence of any natural scale length, not of the Coulomb plastic rheology; basal traction simply scales with the thickness of the wedge, that is, the weight of the rock column above. In the absence of special local processes, a linear basal traction is generally applicable also to a uniform elastic wedge. With the assumption of a constant pore fluid pressure ratio, linear boundary tractions must lead to linear distributions of stress and fluid pressure, such that the effective basal normal stress is also linear. We use a constant gradient a to describe this distribution

$$\bar{\sigma}_n = \sigma_n + P_f = -a\rho g x \tan\theta \tag{9}$$

Here $\bar{\sigma}_n$ at distance x is expressed as a fraction (a) of the weight of the rock column (in the y direction) above. Under conditions that may introduce scale lengths, boundary tractions and thus stresses within the wedge may deviate from a linear distribution. We will briefly discuss the effects of a quadratic boundary traction in section 4.1.

[9] Obviously, $\sigma_x = \sigma_y = -\rho_w g D_0$ at the wedge tip ($x = y = 0$) (Figure 1). Because of the linear boundary conditions, stresses σ_x or σ_y within the wedge must be linear functions of x and y but with a constant term $-\rho_w g D_0$. Therefore the lowest-order terms in stress function $\Phi(x, y)$ must be of the form $\rho_w g D_0 x^2$ and $\rho_w g D_0 y^2$. The following function is thus considered:

$$\Phi = -\frac{1}{2}\rho_w g D_0 (x^2 + y^2) + \frac{\rho g}{2}(k_1 x^2 y + k_2 x y^2) + \frac{\rho g}{6}(k_3 x^3 + k_4 y^3) \tag{10}$$

where k_i (i = 1, 4) are constants to be determined from boundary conditions. According to (2), stresses are derived from Φ as

$$\sigma_x = -\rho_w g D_0 + (k_2 + \sin\alpha)\rho g x + k_4 \rho g y \tag{11a}$$

$$\sigma_y = -\rho_w g D_0 + k_3 \rho g x + (k_1 - \cos\alpha)\rho g y \tag{11b}$$

$$\tau_{xy} = -\rho g (k_1 x + k_2 y) \tag{11c}$$

Using (5), we immediately obtain $k_1 = 0$ and $k_3 = (\rho_w/\rho)\sin\alpha$.

[10] The two remaining unknown constants k_2 and k_4 can be determined from the basal boundary condition. The relationship between boundary tractions and internal stresses along the basal boundary is

$$\sigma_n = \sigma_x \sin^2\theta + \sigma_y \cos^2\theta - \tau_{xy}\sin 2\theta \tag{12a}$$

$$\tau_n = -\frac{1}{2}(\sigma_x - \sigma_y)\sin 2\theta + \tau_{xy}\cos 2\theta \tag{12b}$$

Combining (3b), (4), (8), (9), (11), and (12), we obtain

$$[3k_2 + k_4\tan\theta + (1 - \rho_w/\rho)\sin\alpha] \cdot \sin^2\theta + (\lambda\tan\theta - \sin\theta\cos\theta)\cos\alpha = -a\tan\theta \tag{13a}$$

$$(k_2\tan\theta - k_4 - \cos\alpha)\sin^2\theta - \left[k_2 + \frac{1}{2}(1 - \rho_w/\rho)\sin\alpha\right] \cdot \sin 2\theta = \mu_b' a \tan\theta \tag{13b}$$

k_2 and k_4 can be readily determined from equations (13a) and (13b) as

$$k_2 = \frac{-a(1 - \mu_b'\tan\theta) + (1 - \lambda)\cos\alpha}{\tan\theta} \tag{14a}$$

$$k_4 = \frac{a[3(1 - \mu_b'\tan\theta)\cos^2\theta - 1]}{\sin^2\theta} - \frac{2(1 - \lambda)\cos\alpha}{\tan^2\theta} - \lambda\cos\alpha - \frac{(1 - \rho_w/\rho)\sin\alpha}{\tan\theta} \tag{14b}$$

From (11b) and (3b), the pore fluid pressure is found to be

$$P_f = \rho_w g D + \lambda\rho g y\cos\alpha \tag{15}$$

From (4), (11), and (15), the effective stresses are found to be

$$\bar{\sigma}_x = [k_2 + (1 - \rho_w/\rho)\sin\alpha]\rho g x + (k_4 + \lambda\cos\alpha)\rho g y \tag{16a}$$

$$\bar{\sigma}_y = -(1 - \lambda)\rho g y\cos\alpha \tag{16b}$$

$$\tau_{xy} = -k_2 \rho g y \tag{16c}$$

with k_2 and k_4 given in (14). Given geometry and material properties, there is only one free parameter, a, in the above solution. Comparisons with other relevant solutions are provided in Appendix A. A solution can also be obtained for a quadratically distributed basal traction (Appendix B).

[11] Solution (16) has a very similar form to the exact stress solution of *Dahlen* [1984] for a uniform critical Coulomb wedge. In fact, the $\bar{\sigma}_y$ expression is identical with that of the critical wedge solution. Similar to the critical wedge solution, an important property is that along any straight line radiating from the toe of the wedge, the effective stresses simply scale with x, since $y = x\tan\gamma$, where γ is the angle between the line and the upper surface. The fundamental mechanics is thus independent of the wedge size. This is also a demonstration of the absence of any natural scale length.

2.2. Finite Elastic Wedge

[12] The elastic wedge has been assumed to be infinite in deriving (16), but the solution is applicable to finite wedges as well. On a planar wedge back oriented at an arbitrary angle ϕ with the x axis (Figure 1b), the normal and shear tractions can be determined from internal stresses using (12) if θ in that equation is replaced with $(180° - \phi)$, so that

$$\bar{\sigma}_n = [k_2 + (1 - \rho_w/\rho)\sin\alpha]\rho g x \sin^2\phi + [k_2 \sin 2\phi + k_4 \sin^2\phi + (\lambda - \cos^2\phi)\cos\alpha]\rho g y \tag{17a}$$

$$\tau_n = -\frac{1}{2}[k_2 + (1 - \rho_w/\rho)\sin\alpha]\rho g x \sin 2\phi - \left[k_2\cos 2\phi + \frac{1}{2}(k_4 + \cos\alpha)\sin 2\phi\right]\rho g y \tag{17b}$$

If $\phi = 90°$, (17a) and (17b) reduce to the forms of (16a) and (16c) , respectively. Here we have first obtained the stress solution using prescribed basal boundary conditions and then determined tractions along the wedge back accordingly. Conversely, we could begin with a finite wedge, specify wedge-back tractions to derive the stress solution first, and use the solution to obtain the appropriate basal tractions, as was the approach of *Yin* [1993]. Note that the linear distribution as described by (17) is by no means the only traction distribution for a finite wedge in nature. Depending on the local geological condition, we may prescribe a different boundary condition at the wedge back

and derive a solution different from (16). However, the linear distribution of (17) is the only distribution to yield a solution that satisfies (9) and (8) as well.

[13] Of special interest is the line radiating from the wedge toe at angle

$$\gamma_P = \tan^{-1}\left(\frac{\tan\theta}{3}\right) \tag{18}$$

with the upper surface. At the intersection of this line with the wedge back (point P in Figure 1b), the effective normal traction on the wedge back does not depend explicitly on μ_b''. In other words, given basal normal traction (a), $\bar{\sigma}_n$ at point P does not change with basal shear traction. We call this line the pivot line and point P the pivot point. At the pivot point,

$$\bar{\sigma}_n = \frac{\rho g L \sin^2\phi}{3}\left[-\frac{2a\tan\phi}{(\tan\phi-\tan\theta)\sin 2\theta}+2\left(1-\frac{\rho_w}{\rho}\right)\sin\alpha + (1-\lambda)\cos\alpha\left(\frac{1}{\tan\phi}+\frac{1}{\tan\theta}\right)\right] \tag{19}$$

where L is the distance from the wedge toe to the top edge of the wedge back. The three terms in this expression, in the order shown, represent the effects of basal normal traction, water load on the surface slope, and pore fluid pressure within the wedge.

[14] The pivot point will be useful for our subsequent analysis. It also provides other practical convenience. For example, given λ, we may wish to use a known linear function $\bar{\sigma}_n(y)$ at the wedge back to find matching values of a and μ_b'' for the basal fault. In this case, we can use the value of $\bar{\sigma}_n(y)$ at the pivot point with (19) to determine the value of a, and use $\bar{\sigma}_n(0)$ with (17a) to determine the value of k_2. μ_b'' can then be obtained from (14a).

3. Bending-like Behavior of Elastic Wedges

[15] A number of geological examples of coexistence of extensional and compressive structures in wedge-shaped fault blocks have been provided by *Yin* [1993] and *Yin and Kelty* [2000]. Geological structures such as faults usually represent permanent deformation to which elastic models may not be directly applicable. However, an elastic model can help us infer the prevalent stresses and boundary forces prior to and eventually leading to the permanent deformation. Even in the presence of plastic yielding and faulting, an elastic stress solution for small changes in boundary conditions would approximately predict the sense of deformation and fault slip in response to the incremental stress change. This is why elastic models are widely used in the study of lithospheric stresses in spite of the fact that the mechanics of the lithosphere is better described using a Coulomb plastic behavior as depicted by the Byerlee's law [*Byerlee*, 1978; *Kirby and Kronenberg*, 1987]. On the other hand, to model the complete deformation history of a system, appropriate inelastic rheology should be used.

[16] When the theory of elastic plate bending is applied to the flexure of Earth's lithosphere, such as at subduction zones, stresses are referenced to a background state such as the lithostatic state. The rock is said to be under lateral tension or compression if the horizontal compressive stress is less or greater, respectively, than the reference value. We usually assume that the background stress can be subtracted from the total stress and, after such subtraction, deal with stress perturbations associated with flexure only. One may choose to do the same for an elastic wedge, but the problem is that the definition of a background state necessarily depends on the specific geometry and other parameters of the wedge. Therefore we decide not to attempt to remove a background state for wedges.

[17] We define lateral tension to be a stress state in which the least compressive principal stress (σ_1) is oriented at less than 45° with the upper surface (x axis), and lateral compression to be a state in which σ_1 is at more than 45° with the upper surface. Accordingly, we define the neutral state to be the stress state in which the principal stresses are exactly at 45° with the upper surface. If the upper and lower parts of the wedge have opposite stress states, the line dividing regions of tension and compression is called the neutral line. That the neutral line, if present, must radiate from the toe of the wedge is due to the scale independence of the stress field discussed at the end of section 2.1. The neutral line in our elastic wedge is reminiscent of the neutral plane in a flexed elastic plate (beam). When the whole wedge is in tension or compression, the neutral line is either on the upper or lower surface or "outside of the wedge". For small surface slopes, the tension or compression state is generally inducive to normal or reverse faulting, respectively. For large surface slopes, our tension/compression does not necessarily correspond to normal/reverse faulting as defined in structural geology.

[18] In our coordinate system (Figure 1), both principal stresses along the neutral line are at 45° with the x axis, or equivalently, $\sigma_x = \sigma_y$. Using (11) or (16), we obtain the angle of the neutral line with the upper surface

$$\gamma_N = \tan^{-1}\left(-\frac{k_2+(1-\rho_w/\rho)\sin\alpha}{k_4+\cos\alpha}\right) \tag{20}$$

Note that a neutral state does not generally imply an isotropic state of $\sigma_1 = \sigma_3$. If the neutral line is at the upper surface ($\gamma_N = 0$), it is also a line of isotropic stress. Given wedge geometry, λ, and a, only one specific choice of μ_b'' value can cause isotropic stress in the whole wedge.

[19] We now consider the special stress states in which the neutral line is at the upper ($\gamma_N = 0$) or lower ($\gamma_N = \theta$) surface of the wedge. These states define the transition between states of whole wedge tension or compression and those of coexistent tension and compression. For $\gamma_N = 0$, we have from (20) the following equation:

$$a = \frac{(1-\lambda)\cos\alpha+(1-\rho_w/\rho)\sin\alpha\tan\theta}{1-\mu_b''\tan\theta/(1-\lambda)} \tag{21}$$

For $\gamma_N = \theta$, we have

$$a = \frac{(1-\lambda)\cos\alpha}{1-\mu_b''\tan 2\theta/(1-\lambda)} \tag{22}$$

Figure 2 shows examples of the relation between the two basal parameters a and μ_b'' for (21) (solid line) and (22)

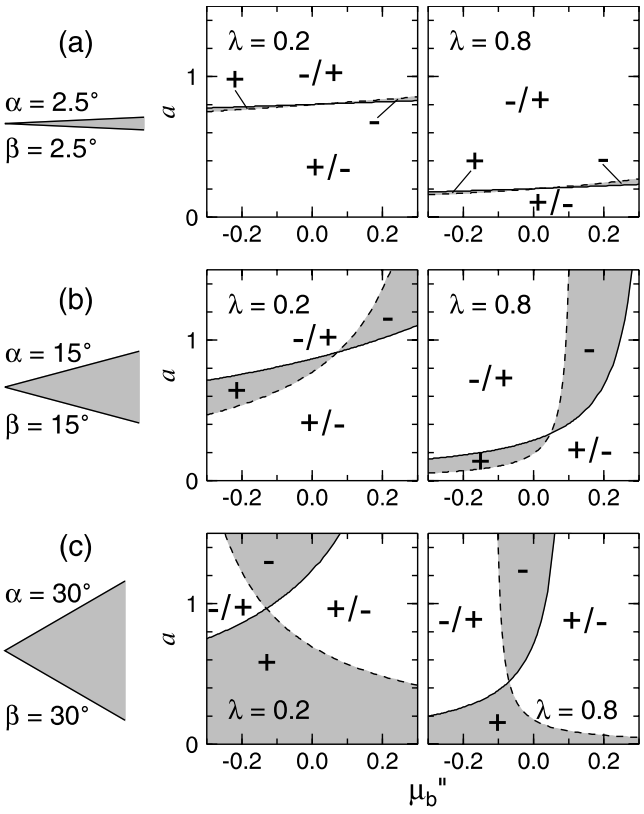

Figure 2. The $a - \mu_b''$ plots for three wedge geometries and two λ values. Values of basal traction parameters a and μ_b'' required to make the upper or basal boundary a neutral line are shown with the solid or dashed lines, respectively. The two curves divide the $a - \mu_b''$ space into four regions: coexistent upper tension and lower compression (plus/minus), coexistent upper compression and lower tension (minus/plus), whole wedge tension (plus), and whole wedge compression (minus).

(dashed line), assuming $\rho_w/\rho = 0.37$. Combinations of three geometries $\alpha = \beta = 2.5°$, 15°, and 30° and two λ values 0.2 and 0.8 result in six examples. For generality, we have also included negative μ_b'' values so that the basal boundary can be either a reverse fault or a normal fault. The two curves divide the $a - \mu_b''$ space into four regions: coexistent upper tension and lower compression (plus/minus), coexistent upper compression and lower tension (minus/plus), whole wedge tension (plus), and whole wedge compression (minus). At the crossover of the two curves, the whole wedge is in a neutral state. The values of a required to achieve the whole wedge neutral state decreases with increasing λ. It can be shown that in both "plus/minus" and "minus/plus" regions and very far from the "plus" or "minus" region, γ_N approaches γ_P.

[20] The mechanics of the four regions can be easily understood by remembering that a and μ_b'' define the magnitude of the normal and shear basal tractions, respectively. To facilitate discussion, we qualitatively consider torque balance around the pivot point of an arbitrary wedge back (Figure 3). Torques generated by the gravitational force, basal normal traction, and basal shear traction must be balanced by the linear distribution of stress $\bar{\sigma}_n$ along the wedge back. The equivalent lines of action of these forces with respect to the pivot point are schematically illustrated in Figure 3. The sign of wedge-back $\bar{\sigma}_n$ is related to lateral tension and compression as defined above.

[21] For small a and large μ_b'', the upper part of the wedge is under tension and the lower part is under compression. For flatly lying thin wedges in Figures 2a and 2b, a smaller a represents less basal support for the weight of the wedge thus permits a greater positive bending force (i.e., causing concave downward flexure), inducive to upper tension and lower compression. The triangular hanging beam discussed in Appendix A is a limiting example ($a = 0$) for this situation. A larger μ_b'' increases shear traction at the lower boundary and hence the bending force, also tending to enhance upper tension and lower compression. Large a or small (or negative) μ_b'' values have the opposite effect.

[22] For some combinations of a and μ_b'' (shaded regions), the neutral line is outside of the wedge ($\gamma_N < 0$ or $\gamma_N > \theta$). In these cases, a larger a or μ_b'' tends to put thin wedges (Figures 2a and 2b) in compression, but the basal traction must be properly sized and oriented for this to happen. For a very thin wedge ($\alpha + \beta = 5°$), only an extremely narrow range of a values can keep the whole wedge in compression, but a wide range of μ_b'' is allowed because even a large basal shear traction results in a small torque due to the small distance of its equivalent line of action from the pivot point (Figure 3). For a thicker wedge ($\alpha + \beta = 30°$), especially with large λ values, the effect is the opposite, and the bending-like behavior is more sensitive to μ_b'' than to a. For thin wedges (Figures 2a and 2b), the region of whole wedge tension is very sensitive to basal normal traction but relatively insensitive to basal shear traction.

[23] A thicker wedge on a thrust basal fault tends to develop upper tension (Figure 2c). Because of the large angle of the basal shear with the upper surface, the wedge has a great tendency to be in a state of whole wedge tension if a is small. Thick wedges are not the focus of this study and will not be further discussed.

[24] In Figure 4, we show $a - \mu_b''$ plots for a wedge with $\alpha + \beta = 15°$ but different orientations with respect to gravity. With the decrease in surface slope, gravity plays an increasingly larger role in compressing the wedge, and therefore it becomes increasingly difficult to put the whole wedge in tension using basal boundary conditions.

4. A Reworked Example

4.1. Wedge Model for Mauna Loa–Kilauea Rift Flank

[25] A rather representative example of bending-like behavior of an elastic wedge has been provided by *Yin*

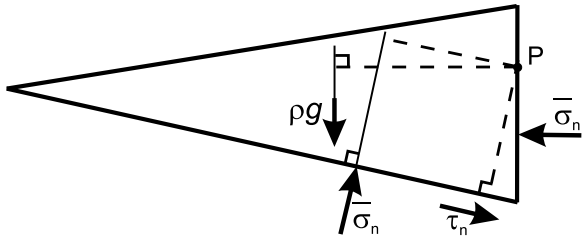

Figure 3. Schematic illustration of torque balance for a finite elastic wedge with respect to the pivot point.

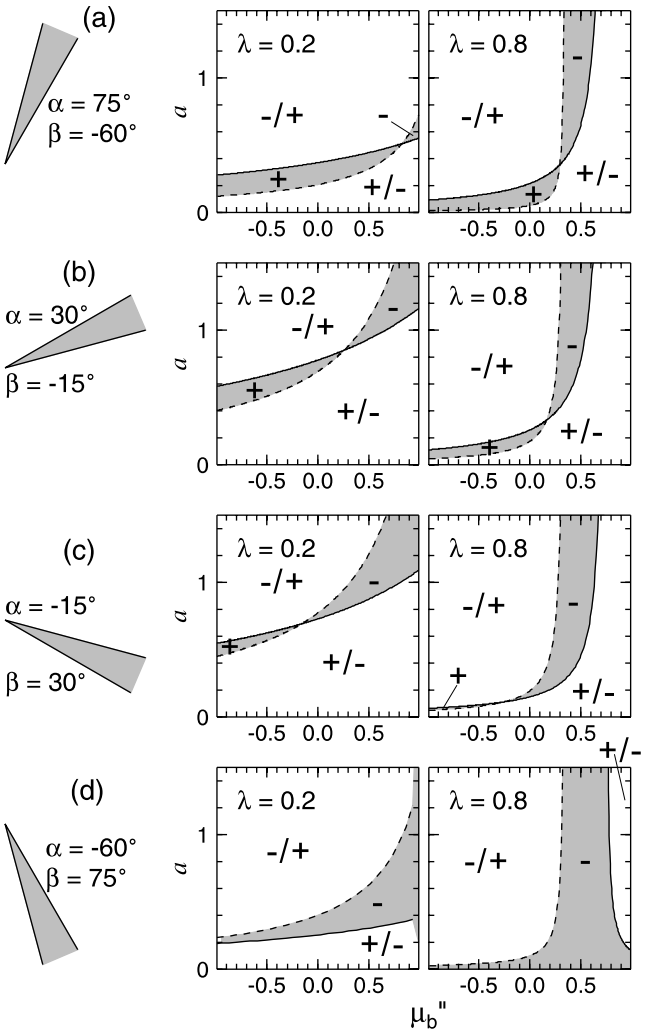

Figure 4. The $a - \mu_b''$ plots similar to those in Figure 2 but for a wedge with $\alpha + \beta = 15°$ at various orientations with respect to gravity. Two λ values 0.2 and 0.8 are shown for each orientation.

and Kelty [2000] using the almost triangular cross section of the Mauna Loa–Kilauea rift flank in Hawaii (Figure 5). Here we reexamine this example using our new solution. The rift flank was formed as a result of upwelling and emplacement of magmas during the development of the Hawaii volcanic island chain. Magma emplacement is still taking place in the rift zone (Figure 5). As reviewed by *Yin and Kelty* [2000], several mechanical models have been used to explain the coeval development of normal faulting in the upper part and reverse faulting in the lower part of this system, but the model of a bent elastic wedge appears to be the most simple and intuitive. The reader is referred to *Yin and Kelty* [2000] for other geological details.

[26] Following *Yin and Kelty* [2000], we use a surface slope and basal dip of 7° and 3°, respectively, and a wedge length of L = 60 km, but instead of a wedge back perpendicular to the upper surface (ϕ = 90°) we use a vertical wedge back (ϕ = 97°). We also assume the densities of the submarine wedge and overlying water to be 2700 kg/m^3 and 1000 kg/m^3, respectively. "Free" parameters to be determined are pore fluid pressure ratio within the wedge (λ), basal traction gradient (a), and basal friction property (μ_b'').

4.2. Parameter Range and Reference Model

[27] The primary objective of studying this example is to explore the feasibility of the concept of a "bent wedge", not to determine precise parameter values. As shown in section 3, an infinite number of combinations of parameter can result in a bending-like behavior. The $a - \mu_b''$ plot in Figure 6 for the Mauna Loa–Kilauea rift flank geometry with $\lambda = 0.8$ partially illustrates the situation. Numerous μ_b'' values combined with some small a may result in tension in the upper part and compression in the lower part.

[28] In order to limit our options within a physically reasonable range, we make the assumption that the "natural" state of the wedge is that of a critically tapered Coulomb wedge, and states of stress featuring coexistent tension and compression are variations from this reference state. We choose the critical wedge as a reference state because it represents a natural balance of rock strength, gravitational force, and all boundary tractions in a wedge-shaped body. It is similar to assuming a reference state of

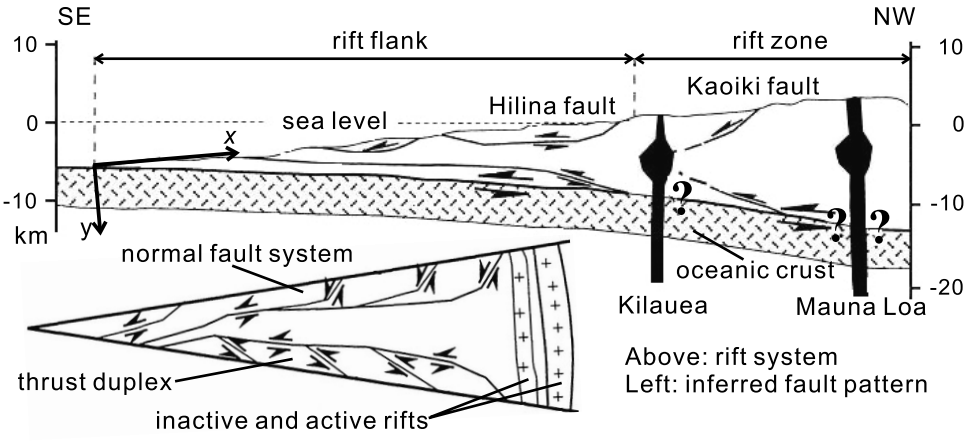

Figure 5. Cross section of Mauna Loa–Kilauea rift flank in Hawaii and fault pattern inferred by *Yin and Kelty* [2000]. Based on *Yin and Kelty* [2000].

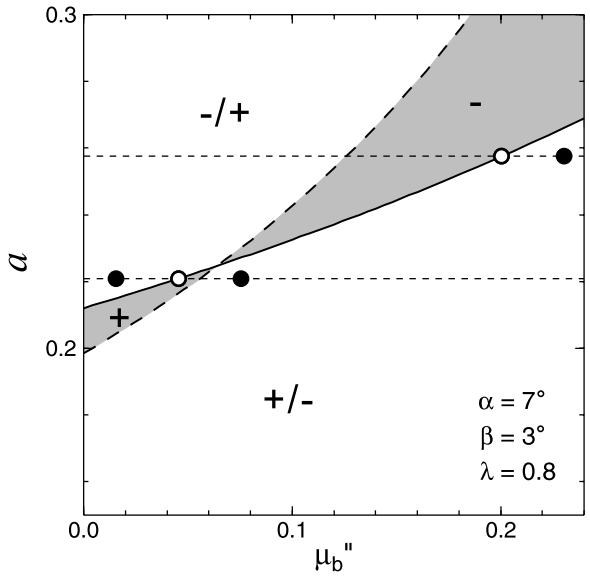

Figure 6. The $a - \mu_b''$ plot for the Mauna Loa–Kilauea wedge model with $\lambda = 0.8$. See Figure 2 for meaning of the plus/minus signs. The two critical states mentioned in section 4.2 are indicated by open circles. Cases discussed in section 4.3 are indicated by solid circles, except for the case of $\mu_b'' = 0.5$.

stress based on the Byerlee's law [*Byerlee*, 1978] when modeling regional tectonic stresses in the lithosphere. We further assume that the critical wedge has been formed with an internal friction of 1.1 [*Dahlen*, 1984]. The value is considered reasonable for crustal rocks [*Davis et al.*, 1983; *Dahlen*, 1984], but the exact number is less important given its trade-off with all the other parameters.

[29] Given wedge geometry, internal friction, and pore fluid pressure ratio, there are two critical states, each corresponding to a specific μ_b'' value [*Dahlen*, 1984]. In the critical state with a smaller μ_b'', the whole wedge is on the verge of gravitational collapse. In the other state, with a larger μ_b'', the whole wedge is on the verge of compressive failure. It can be shown that stresses in a critical wedge can be exactly described using our elastic wedge solution [*Wang and Hu*, 2006], and each of the two critical μ_b'' values is accompanied by a unique a value. Since the top surface is the neutral line ($\bar{\sigma}_x = \bar{\sigma}_y = 0$) for a noncohesive critical wedge, the two critical states both fall on the solid line in Figure 6 (open circles), on either side of the whole wedge neutral state (crossover of the two curves). We require stress solutions for a bent elastic wedge to have pairs of a and μ_b'' close to these critical values. Too large a deviation from the critical values increases the risk of assuming unphysical geological conditions. For a flatly lying thin wedge, the basal normal traction is determined mainly by the weight of the rock column above. Given pore fluid pressure ratio, the effective basal normal traction (represented by parameter a in equation (9)) thus should not vary much, as reflected by the small difference between the two critical a values. We therefore decide to fix a at a critical value and vary the basal shear traction by slightly deviating μ_b'' from its critical value. A change in μ_b'' can be due to a change in μ_b but, in the case of a volcanic rift flank, more likely due to a change in basal pore fluid pressure as controlled by the evolution of hydrogeological conditions. Fixing μ_b'' but varying a instead would serve the same purpose in terms of achieving the primary objective of studying this example.

[30] If λ is allowed to vary, there is still a wide range of choices of critical a and μ_b'' values. It is convenient to use the effective normal traction ($\bar{\sigma}_n$) at the pivot point of the wedge back to illustrate this problem (equation (19)). The values of $\bar{\sigma}_n$ at this point as functions of a for different λ values are shown in Figure 7. The two critical a values are also shown for each λ. In accordance with intuition, $\bar{\sigma}_n$ on the vertical wedge back for the whole wedge tension critical state is slightly compressive for all λ values. Obviously, we must specify λ in order to chose the value of a. We decide to use the frequently assumed [e.g., *Dahlen*, 1984] moderately high value of 0.8, but if independent constraints become available in the future, the results can be readily updated using a different λ value. The choice of λ may appear to be quite arbitrary at this stage, but it will become clearer at the end of section 4.3 why very low λ values are less preferred.

[31] The elastic wedge theory of stable versus critical Coulomb wedges has been presented in a separate paper [*Wang and Hu*, 2006]. Here it suffices to report that for the whole wedge tension critical state with all the above parameters, $a = 0.221$ and $\mu_b'' = 0.0456$, and for the whole wedge compression critical state, $a = 0.258$ and $\mu_b'' = 0.200$ (Figure 6). It can be easily verified that these μ_b'' values are required by the critical taper solution of *Dahlen* [1984]. These are the two reference models we use.

4.3. Results

[32] We first use the whole wedge tension critical state as the initial reference state. This is to assume that the wedge had been on the verge of gravitational collapse before a change in the basal condition. Effective principal stresses in

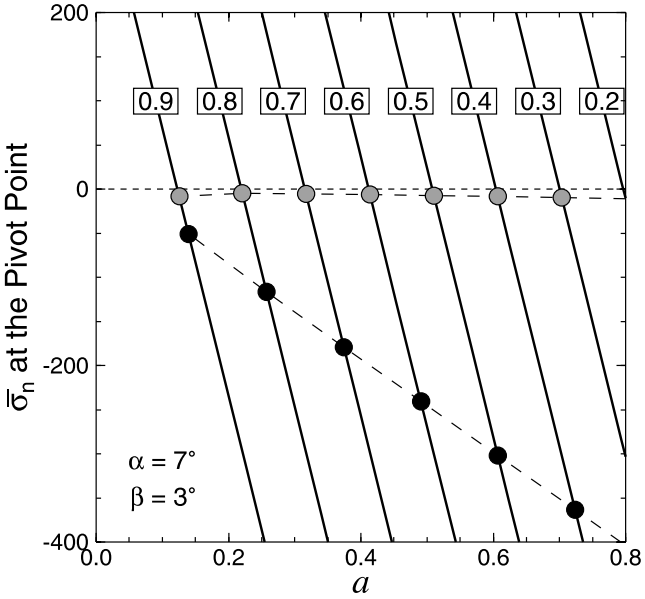

Figure 7. Effective normal traction at the pivot point of the back of the Mauna Loa–Kilauea wedge model as a function of a for different λ values (numbers in panes). Grey and dark dots for each λ indicate extensionally and compressively critical states, respectively.

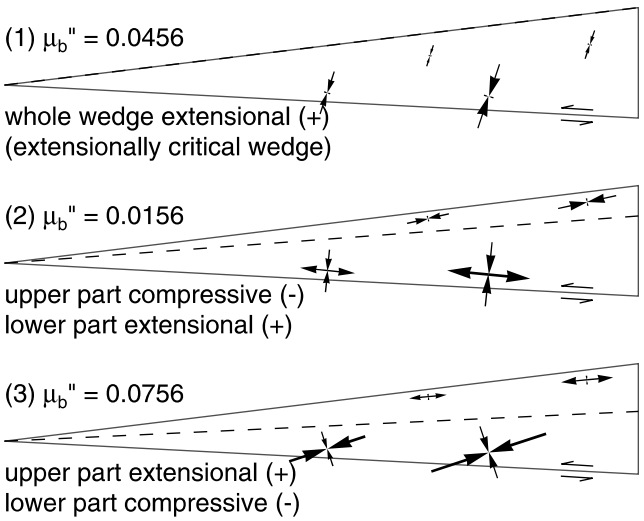

Figure 8. Effective principal stresses in the $\lambda = 0.8$ Mauna Loa–Kilauea wedge models with the extensionally critical wedge ($a = 0.221$; case 1) as the reference model. Cases 2 and 3 are derived by changing μ_b'' by ±0.03 from its critical value. The dashed line in each case represents the neutral line. The three states in the $a - \mu_b''$ space are shown in Figure 6.

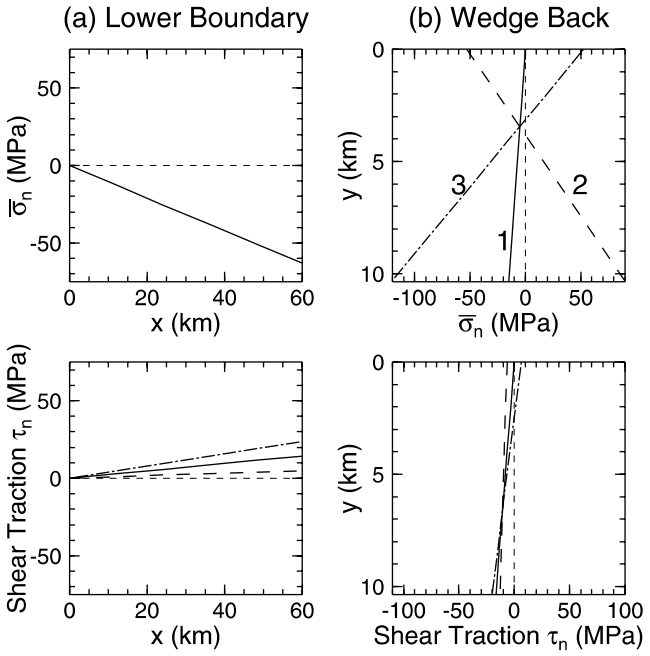

Figure 9. Tractions along (a) the lower boundary and (b) the wedge back for the three models shown in Figure 8. Solid, dashed, and dot-dashed lines correspond to cases 1, 2, and 3 in Figure 8, respectively, with case 1 being the reference state. The effective basal normal traction is the same for all three cases.

this reference state are shown in Figure 8 (case 1). Decreasing or increasing μ_b'' by a small amount such as 0.03 puts the wedge into regions of coexistent tension and compression (Figure 6). The effective principal stresses for these states (cases 2 and 3) are shown in Figure 8 in comparison with the reference state. The greater μ_b'' value (case 3) yields the desired state of coexisting upper tension and lower compression.

[33] Tractions along the basal and back boundaries for all the three cases in Figure 8 are shown in Figure 9. With a fixed, all three cases have the same effective basal normal traction, but different μ_b'' values result in different basal shear tractions (Figure 9a). The most illuminating is the effective normal traction distribution $\bar{\sigma}_n$ on the wedge back (Figure 9b), although the sign of $\bar{\sigma}_n$ does not exactly correspond to tension or compression as defined in section 3. All $\bar{\sigma}_n$ lines intersect at the pivot point (equation (19)). Bending-like behavior of the wedge is indicated by any deviation from the reference $\bar{\sigma}_n$. Any increase in basal shear traction will cause tension (and positive $\bar{\sigma}_n$) along the top of the wedge. Owing to the use of the critical wedge as a reference model, shear traction along the wedge back is small for all three cases, a situation intuitively reasonable for the rift zone.

[34] Using other μ_b'' values changes the position of the neutral line. To illustrate the sensitivity of neutral line position to basal shear traction, we show the angle of the neutral line with the upper slope γ_N (equation (20)) as a function of μ_b'' in Figure 10. Figure 10 again illustrates the ease with which tension and compression can coexist in a flatly lying thin wedge. In the case shown, any μ_b'' greater than 0.056 will cause coexistent upper tension and lower compression, the model we wish to create for Mauna Loa–Kilauea. On the other hand, any value less than 0.0456, including negative values that represent a normal basal fault, will cause the opposite effect. For the specific a value chosen in this example, whole wedge tension occurs only for a narrow range of μ_b'' values. Away from this range in either direction, the position of the neutral line asymptotically approaches that of the pivot line. Whole wedge compression never occurs for this a value.

[35] It is equally easy to create coexistent upper tension and lower compression if we instead use the whole wedge com-

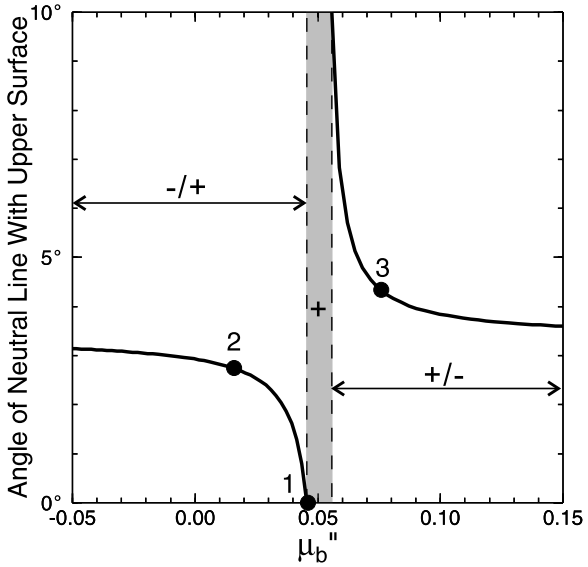

Figure 10. Angle of the neutral line γ_N with the upper surface as a function of μ_b'' in Mauna Loa–Kilauea wedge models with $\lambda = 0.8$ and $a = 0.221$ (see Figure 6 for position in the $a - \mu_b''$ space). Labeled dots correspond to the three cases in Figure 8. See Figure 2 for the meaning of plus/minus signs.

pression critical wedge as the reference model (Figure 11). Increasing μ''_b by 0.03 puts a narrow near-surface part of the wedge in tension (case 2 in Figure 11a). A much large increase such as $\mu''_b = 0.5$ will move the neutral line down to a mere 3° from the upper surface (case 3 in Figure 11a). The small size of the upper zone of tension can be qualitatively explained by looking at the wedge back $\bar{\sigma}_n$ distribution, shown in Figure 11b as an inset. Tensile $\bar{\sigma}_n$ occurs above the crossover of the $\bar{\sigma}_n$ profile with the zero stress line (short-dashed vertical line). Because $\bar{\sigma}_n$ at the pivot point is much more compressive for this reference state, the upper segment of tension tends to be very small even for a large basal shear traction.

[36] Similar results can be obtained using other λ values, but very small λ values are less preferred. The pivot point $\bar{\sigma}_n$ for a compressively critical wedge becomes more compressive as λ decreases (trajectory of black dots in Figure 7). If a very compressive critical wedge is used as the reference, larger μ''_b values are needed to create a sizable upper portion of tensile $\bar{\sigma}_n$ as can be inferred from the case in Figure 11. The problem with using too large a μ''_b is that the stresses will deviate very far from the reference state. It can be shown that for $\lambda < 0.482$, an extensionally critical wedge is present only if the basal fault is a normal fault ($\mu_b < 0$) for this wedge geometry. A normal basal fault is unlikely to be relevant to the Mauna Loa–Kilauea rift flank.

4.4. Discussion

[37] As discussed near the beginning of section 3, an elastic stress solution is useful for predicting the sense of incremental deformation caused by small changes in boundary conditions, even in the presence of faulting. The question is whether the incremental stress change will actually lead to new faults. For example, if normal faults have already developed in the reference state shown in case 1 of Figure 8, although tension in the upper part of the wedge in case 3 of Figure 8 may cause greater displacements on these faults, the compressive stress in the lower part may not be large enough to develop new faults. Note that the lateral compressive stress (e.g., as represented by $\bar{\sigma}_n$ at the wedge back) in the lower wedge (Figure 9b) is less than that of a compressively critical state (case 1 in Figure 11b inset) which is the theoretically required minimum to develop thrust faults in the wedge. Direct comparison of the predicted stresses to fault patterns in the lower part of the wedge in Figure 5 may thus be in question.

[38] One solution to this problem is to assume the compressively critical state to be the initial reference state. In this case, thrust faults would have already been developed in the wedge. An increase in μ''_b and hence greater compression to the lower wedge, such as in either case 2 or case 3 of Figures 11a, would cause greater displacements on these faults. We can also speculate that because the low Coulomb strength, material near the surface (seafloor) would not be able to sustain significant lateral tension, and thus extensional failure such as normal faulting would likely occur in the upper wedge. In this context, the compressively critical state may be a better reference model to consider. That the segment of tension in this purely elastic model is too thin such as in case 2 of Figure 11a may not present a problem in reality if a longer deformation history is considered. In a real wedge, faulting would weaken the very top part of the wedge, such that the lateral tension would occur to a somewhat larger depth.

[39] Another solution is to resort to material heterogeneity in a real wedge. Although the compressive stress in the lower wedge of case 3 of Figure 8 may not exceed failure stress for a uniform, intact wedge, some existing weak planes with optimal orientation for failure and locally very high pore fluid pressure may fail under relatively small stress and cause limited thrust faulting.

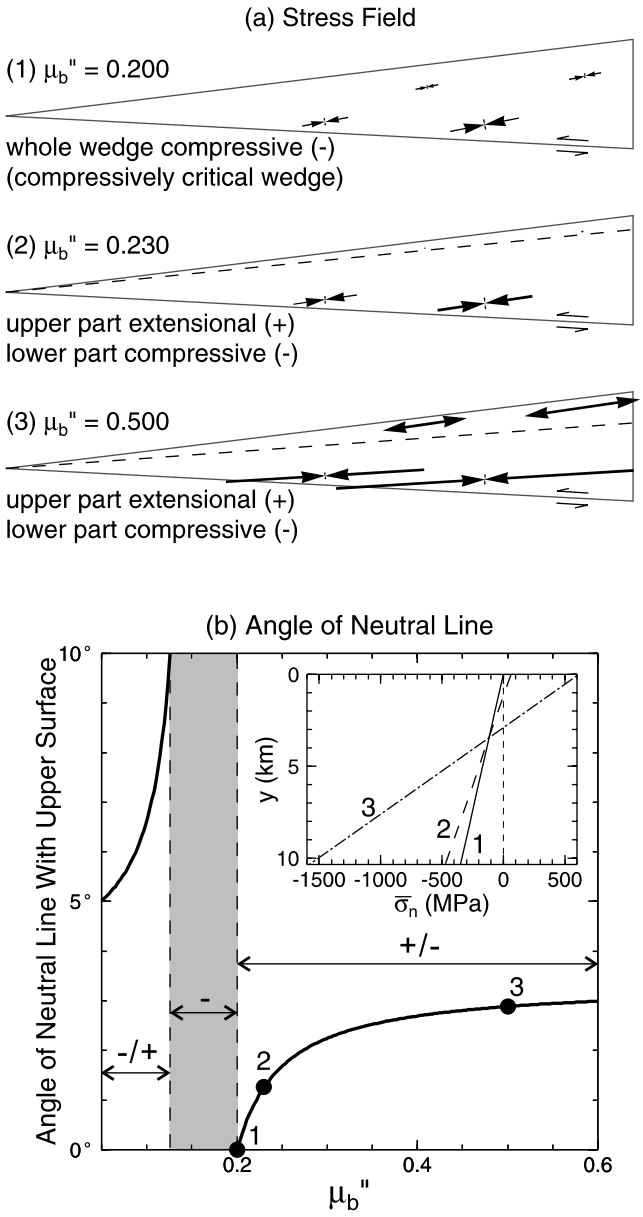

Figure 11. Results of Mauna Loa–Kilauea wedge models with the $\lambda = 0.8$ compressively critical wedge ($a = 0.258$) as the reference model. (a) Effective principle stresses. Case 1 is the reference state. The neutral line is indicated by a dashed line in each case. Cases 1 and 2 are shown in the $a - \mu''_b$ space in Figure 6. (b) Angle of the neutral line γ_N with the upper surface as a function of μ''_b. Labeled dots correspond to the three cases in Figure 11a. Inset shows wedge-back effective normal tractions for the three cases.

[40] Our results above have demonstrated that the coexistence of lateral tension and compression is the most common state for thin elastic wedges. In fact, it is difficult not to have such coexistence. One would have to find a subtle balance of parameters to be able to put the whole wedge into compression or tension, and any small change in basal condition can easily break the balance. Our results thus removed the stringent conditions put forth by *Yin and Kelty* [2000] to cause the bending-like behavior. Specifically, the pore fluid pressure ratio within the wedge or along the basal fault does not have to be as high as 0.9–0.95, and special magma emplacement processes are not required. The robustness of the bending-like behavior may have implications for many other geological problems involving wedge-shaped fault blocks.

[41] In applying the solutions to Mauna Loa–Kilauea, we have followed the geological analyses of *Yin and Kelty* [2000], who dismissed the geological model of whole wedge extension. If such model holds, it can be modeled using a whole wedge tension stress model such as case 1 in Figure 8.

[42] In the above, we have only considered an elastic wedge with a linear distribution of basal traction. Situations may arise that require the consideration of nonlinear boundary tractions. For example, to account for the vertical variation of the density of magma, assumed to be located at the back of the Mauna Loa–Kilauea wedge (Figure 5), *Yin and Kelty* [2000] considered quadratically varying tractions. Their preferred solutions include a small or no quadratic term in the boundary tractions. We do not examine the quadratic boundary conditions in detail in this work but point out some characteristics of the quadratic situation in the following paragraph. Note that although the vertical change may be of some interest, the absolute value of the magma density has no significance in this problem as was also observed by *Yin and Kelty* [2000].

[43] The solution with a quadratic term $bx^2\tan^2\theta$ added to the basal boundary traction is given in Appendix B. From this solution, it is obvious that a quadratic basal traction must lead to a quadratic wedge-back traction, and vice versa. A nonzero b gives rise to constants k_5 and k_6 (B3) thus quadratic terms in all stress components (B2). On the basis of parameters used by *Yin and Kelty* [2000], k_5 is of the order of 10^{-6} m^{-1}, and according to (B3a) b is of the order of 10^{-5} m^{-1}. Over a 10 km high wedge back, the change in $\bar{\sigma}_n$ due to the quadratic term is only a couple of tens of MPa. For such a small effect, results of the linear analyses presented in this paper still qualitatively apply. Moreover, the effect of the magma density variation is probably of second-order importance, considering simplifications made to many other aspects of the problem.

5. Conclusions

[44] We have derived a stress function solution for infinite and finite elastic wedges with a frictional basal boundary. The solution is applicable to a submarine or subareal fault block bounded by a thrust or normal basal fault. We have focused primarily on the situation of linearly distributed boundary tractions but also provided a solution with quadratic boundary tractions.

[45] Using the linear solution, we have explored conditions to cause the bending-like behavior of thin elastic wedges, that is, the coexistence of lateral tension and compression that are vertically divided by a neutral line. Given wedge geometry and pore fluid pressure, different combinations of basal effective normal traction and shear traction may cause coexistent upper tension and lower compression, coexistent upper compression and lower tension, whole wedge tension, or whole wedge compression. The conditions are best illustrated using the $a - \mu_b''$ plots such as those in Figures 2 and 4. We have demonstrated the propensity of elastic wedges, especially of thin wedges, to have a bending-like behavior.

[46] As an example, we have reanalyzed an elastic wedge model for the Mauna Loa–Kilauea rift flank in Hawaii to explain the coeval development of normal faulting in its upper part and reverse faulting in its lower part. Our analysis in principle supports the bent wedge concept of *Yin and Kelty* [2000] for this system, but it reveals the robustness of such a concept by showing that a very wide range of physically reasonable parameters can cause coexistent upper tension and lower compression. For example, in contrast to their conclusions, we did not find a need to limit pore fluid pressures in the wedge and basal decollement to a range of "exceedingly high" values, although very low values such as λ less than about 0.5 are less preferred. Also in contrast to their conclusions, special magma emplacement processes or mechanisms to generate a special vertical distribution of stresses along the rift zone are not required, because the bending-like behavior can be caused by reasonably small changes in basal conditions such as a pore fluid pressure decrease with time. Near a critical state, which is used as the reference state in our analysis, the stress state is very sensitive to basal conditions; a small change in basal traction may cause either coexistent upper tension and lower compression or the opposite. However, slightly away from the critical state, the solution is very insensitive to changes in the basal boundary conditions.

Appendix A: Comparison With Previously Published Elastic Wedge Solutions

[47] Comparison with previously published solutions serves three purposes: (1) It provides a rigorous check for the new solution because a correct general solution should reduce to simpler forms for more specific conditions, (2) it demonstrates how the new solution may be applied to problems that do not have the same boundary conditions as ours, and (3) it provides a critique of previous solutions that contain errors.

[48] A stress solution for a triangular hanging beam (Figure A1a) is available from *Xu* [1979]. To apply our new solution, let $\rho_w = a = \lambda = \alpha = 0$. Therefore $k_2 = 1/\tan\theta$ and $k_4 = -2/\tan^2\theta$. Stresses in the hanging beam are then

$$\sigma_x = \frac{\rho g(x\tan\theta - 2y)}{\tan^2\theta} \tag{A1a}$$

$$\sigma_y = -\rho g y \tag{A1b}$$

$$\tau_{xy} = -\frac{\rho g y}{\tan\theta} \tag{A1c}$$

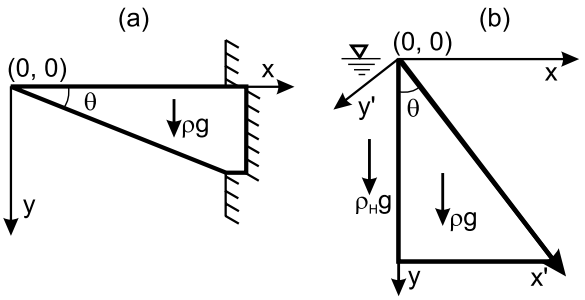

Figure A1. Geometries of two simple problems from *Xu* [1979]. (a) A triangular hanging beam subject to its own weight ρg. (b) A triangular dam subject to water pressure $\rho_H g$ on its vertical side. Coordinate system (x', y') is used with solution (16), and system (x, y) is used by *Xu* [1979].

Equation (A1a) is the solution given by *Xu* [1979]. A more general solution can also be obtained using (16) if $\alpha \neq 0$.

[49] Another solution available from *Xu* [1979] is for a triangular dam subject to water pressure $\rho_H g y$ on its vertical side (Figure A1b). To apply our solution, we need to set up the coordinate system (x', y') as shown in Figure A1b and let $\rho_w = \lambda = \mu_b = 0$. In this system, $\alpha = \theta - 90°$ and $\beta = 90°$. At the "lower" (water side) boundary, $\bar{\sigma}_n = \sigma_n = -\rho_H g x'/\cos\theta$. Comparing this with (9), we obtain $a = \rho_H/(\rho \sin\theta)$. Stresses in the (x', y') system are then

$$\sigma_{x'} = -\frac{\rho_H g x'}{\tan\theta \sin\theta} + \left[\frac{\rho_H(3\cos^2\theta - 1)}{\sin^3\theta} - \frac{\rho\cos\theta}{\tan\theta}\right] g y' \tag{A2a}$$

$$\sigma_{y'} = -\rho g y' \sin\theta \tag{A2b}$$

$$\tau_{x'y'} = -\left[\rho\cos\theta - \frac{\rho_H}{\tan\theta\sin\theta}\right] g y' \tag{A2c}$$

Writing x' and y' in terms of x and y and rotating the coordinate system into (x, y), we obtain the solution given by *Xu* [1979]:

$$\sigma_x = -\rho_H g y \tag{A3a}$$

$$\sigma_y = \left(\frac{\rho}{\tan\theta} - \frac{2\rho_H}{\tan^3\theta}\right) g x + \left(\frac{\rho_H}{\tan^2\theta} - \rho\right) g y \tag{A3b}$$

$$\tau_{xy} = -\frac{\rho_H g x}{\tan^2\theta} \tag{A3c}$$

[50] *Liu and Ranalli* [1992] derived a stress solution for an elastic trapezoid. Although they did not have a frictional basal boundary, their solution can be cast into a form similar to ours if the trapezoid is reduced to a wedge.

[51] Solutions by *Yin* [1993] and *Yin and Kelty* [2000] are for a finite wedge, similar to that in Figure 1b but with $\phi = 90°$. If an arbitrary constant term that violates the basal friction condition is removed from the σ_x expression of *Yin* [1993], his solution should be similar to the solution with linear boundary conditions of *Yin and Kelty* [2000]. Unfortunately, an error in dealing with pore fluid pressure gradient terms $\partial P_f/\partial x$ and $\partial P_f/\partial y$ occurred to both solutions when the stress equilibrium equations were written in terms of effective stresses. For the special case of zero pore fluid pressure, their solutions should have a similar form to ours since the boundary conditions can be shown to be the same as ours. Because their graphical illustrations showed results incompatible with boundary conditions, e.g., basal shear and normal tractions do not agree with friction coefficients in several figures, possibly due to plotting errors, we did not proceed with a more specific comparison.

Appendix B: Solution for Quadratic Distribution of Basal Traction

[52] The formulation of the problem is as described in section 2.1 except that a quadratic term is added to the effective basal normal traction, that is,

$$\bar{\sigma}_n = -\rho g\left(ax\tan\theta + bx^2\tan^2\theta\right) \tag{B1}$$

Using a more complex Airy stress function than (10), we have obtained the following solution:

$$\bar{\sigma}_x = [k_2 + (1 - \rho_w/\rho)\sin\alpha + k_5 x]\rho g x + [k_4 + \lambda\cos\alpha + 2k_6 x - (2 + \lambda)k_5 y]\rho g y \tag{B2a}$$

$$\bar{\sigma}_y = -(1 - \lambda)(\cos\alpha - k_5 y)\rho g y \tag{B2b}$$

$$\tau_{xy} = -(k_2 + 2k_5 x + k_6 y)\rho g y \tag{B2c}$$

where constants k_2, k_4, k_5, and k_6 are determined from boundary conditions, with k_2 and k_4 being identical to those given in (14) and

$$k_5 = \frac{b\left(\tan^2\theta + 4\mu_b'\tan\theta - 3\right)}{3(2 - \lambda) + (2 + \lambda)\tan^2\theta} \tag{B3a}$$

$$k_6 = \frac{k_5}{2}\left(\frac{\lambda}{\sin 2\theta} - \frac{3}{\tan\theta} + \tan\theta\right) - \frac{b}{2\sin 2\theta} \tag{B3b}$$

In this wedge, the pore fluid pressure is

$$P_f = \rho_w g D + (\cos\alpha - k_5 y)\lambda\rho g y \tag{B4}$$

[53] **Acknowledgments.** Comments from Sergei Medvedev helped clarify many points. We thank him, Yongen Cai, and an Associate Editor for reviewing the paper and An Yin for discussions on previous solutions. Geological Survey of Canada contribution 2005678.

References

Byerlee, J. D. (1978), Friction of rocks, *Pure Appl. Geophys.*, *16*, 615–626.

Dahlen, F. A. (1984), Noncohesive critical Coulomb wedges: An exact solution, *J. Geophys. Res.*, *89*, 10,125–10,133.

Dahlen, F. A. (1990), Critical taper model of fold-and-thrust belts and accretionary wedges, *Annu. Rev. Earth Planet. Sci.*, *18*, 55–99.

Davis, D., J. Suppe, and F. A. Dahlen (1983), Mechanics of fold-and-thrust belts and accretionary wedges, *J. Geophys. Res.*, *88*, 1153–1172.

Fung, Y. C. (1965), *Foundations of Solid Mechanics*, 525 pp., Prentice-Hall, Upper Saddle River, N. J.

Kirby, S. H., and A. K. Kronenberg (1987), Rheology of the lithosphere: Selected topics, *Rev. Geophys.*, *25*(6), 1219–1244.

Liu, J. Y., and G. Ranalli (1992), Stresses in an overthrust sheet and propagation of thrusting: An Airy stress function solution, *Tectonics*, *11*, 549–559.

Platt, J. P. (1993), Mechanics of oblique convergence, *J. Geophys. Res.*, *98*, 16,239–16,256.

Wang, K., and J. He (1999), Mechanics of low-stress forearcs: Nankai and Cascadia, *J. Geophys. Res.*, *104*, 15,191–15,205.

Wang, K., and Y. Hu (2006), Accretionary prisms in subduction earthquake cycles: The theory of dynamic Coulomb wedge, *J. Geophys. Res.*, *111*, B06410, doi:10.1029/2005JB004094.

Xu, Z. L. (1979), *Elasticity* (in Chinese), vol. I, 396 pp., People's Educ. Publ. House, Beijing.

Yin, A. (1993), Mechanics of wedge-shaped fault blocks: 1. An elastic solution for compressive wedges, *J. Geophys. Res.*, *98*, 14,245–14,256.

Yin, A., and T. K. Kelty (2000), An elastic wedge model for the development of coeval normal and thrust faulting in the Mauna Loa-Kilauea rift system in Hawaii, *J. Geophys. Res.*, *105*, 25,909–25,925.

Y. Hu, School of Earth and Ocean Sciences, University of Victoria, Victoria, BC, Canada V8P 5C2. (yanhu@uvic.ca)

K. Wang, Pacific Geoscience Centre, Geological Survey of Canada, 9860 West Saanich Road, Sidney, British Columbia, Canada V8L 4B2. (kwang@nrcan.gc.ca)